

PAPER • OPEN ACCESS

Valence charge distribution in homogenous silicon-aluminium thin-films

To cite this article: Annett Thøgersen *et al* 2018 *J. Phys.: Condens. Matter* **30** 335502

View the [article online](#) for updates and enhancements.

Related content

- [A quantitative study of valence electron transfer in the skutterudite compound CoP₃ by combining x-ray induced Auger and photoelectron spectroscopy](#)
S Diplas, Ø Prytz, O B Karlsen et al.
- [Electronic structure studies of Ni-X \(X: B, S, P\) alloys using x-ray photoelectronspectroscopy, x-ray induced Auger electron spectroscopy and density functional theorycalculations](#)
S Diplas and O M Løvrik
- [Formation of nanoporous Si upon self-organized growth of Al and Si nanostructures](#)
Annett Thøgersen, Ingvild J T Jensen, Marit Stange et al.



IOP | ebooks™

Bringing you innovative digital publishing with leading voices to create your essential collection of books in STEM research.

Start exploring the collection - download the first chapter of every title for free.

Valence charge distribution in homogenous silicon-aluminium thin-films

Annett Thøgersen[✉], Ingvild J T Jensen, Marit Stange, Arne Røyset, Ole Martin Løvvik, Alexander G Ulyashin and Spyros Diplas

SINTEF Industry, Forskningsveien 1, 0373 Oslo, Norway

E-mail: annett.thogersen@sintef.no

Received 24 May 2018, revised 24 June 2018

Accepted for publication 9 July 2018

Published 26 July 2018




CrossMark

Abstract

Homogenous $a\text{Si}_{1-x}\text{Al}_x\text{H}_y$ alloyed thin films, made by magnetron sputtering, has been found to exhibit tunable band gap and dielectric constant depending on their composition. The optical properties of alloys are largely defined by their electronic structure, which is strongly influenced by interatomic charge transfer. In this work we have quantified interatomic charge transfer between Si, Al and H in $a\text{Si}_{1-x}\text{Al}_x\text{H}_y$ thin-films, with $x \leq 0.25$ and $y \geq 0$. Charge transfer was found experimentally using x-ray photoelectron spectroscopy, by incorporating Auger parameter data into the Thomas and Weightman model. Both the perfect and imperfect screening models were tested, and the results were compared to models calculated using density functional theory based molecular dynamics. Using imperfect screening properties of Si and Al resulted in an excellent agreement between the experimental and computational results. Alloying aSi with Al is associated with donation of electrons from Al to Si for $y = 0$. For $y > 0$ electrons are transferred away from both Al and Si. The change in Si valence charge increases linearly with increasing band gap and decreasing dielectric constant. These relationships can be used as a quick guide for the evaluation of the Si valence charge and subsequently optoelectronic properties, at specific Al/Si ratios.

Keywords: silicon, aluminium, charge, Auger, XPS

 Supplementary material for this article is available [online](#)


(Some figures may appear in colour only in the online journal)

1. Introduction

Increasing demand for low-cost and non-toxic optoelectronic materials, such as solar cells and light-emitting diodes (LEDs), requires development of new types of materials [1–3]. Hydrogenated amorphous silicon (aSi:H) is currently being used in heterojunction solar cells. Amorphous silicon is abundant, nontoxic, and has a band gap in the appropriate range (1–2 eV). Its high absorption coefficient resulting from the presence of dangling bonds in the structure enables all optical transitions. Passivating the dangling bonds with hydrogen increases the band gap of the material [4]. Amorphous silicon

thin films can be deposited at low temperatures and on large areas, which is important for industrial production of modules on low cost substrates for solar cell applications [5]. However, hydrogenated amorphous silicon suffers from light induced degeneration and hydrogen desorption, also known as the Staebler–Wronski effect. This effect has driven production towards other more expensive and often toxic alternatives.

In a previous work, we have shown that homogenous single phased $a\text{Si}_{1-x}\text{Al}_x$ (aSiAl) and $a\text{Si}_{1-x}\text{Al}_x\text{H}_y$ (aSiAl:H) films can be made via magnetron sputtering [7]. Due to the low solubility of Al in Si, aSiAl alloys with high Al content have not been extensively investigated neither in a structural or an optoelectronic context. To our knowledge; $a\text{Si}_{1-x}\text{Al}_x\text{H}_y$ has not previously been studied for $x > 8.3$ at.% [6]. There is therefore currently a lack of knowledge and understanding of the alloying mechanisms. Changing the stoichiometry of our

 Original content from this work may be used under the terms of the [Creative Commons Attribution 3.0 licence](#). Any further distribution of this work must maintain attribution to the author(s) and the title of the work, journal citation and DOI.

aSiAl and aSiAl:H films resulted in a change in band gap and dielectric constant [7]. In this paper we want to relate the change in band gap and dielectric constant to the interatomic electron charge (re-)distribution between the constituent atoms of the amorphous alloys, namely Al, Si and H. The extent to which charge transfer takes place between atoms affects local electronic structure and determines the nature of their bonding. Different modes of bonding may result in different types of atomic arrangement, which influences the material properties and performance. Understanding the alloying mechanisms of thin film constituents is therefore important before incorporating these films in technological devices, such as solar cells. In this context, charge transfer phenomena are central to understanding alloying behaviour at the atomic level. Data from ellipsometry and UV-vis spectrometry reported in a previous paper [7] was used in order to connect the structural studies with the optoelectronic performance of the films.

The homogenous morphology of the films allows us to study the alloying behaviour of the film constituents by the means of low spatial resolution electron spectroscopy techniques such as x-ray photoelectron spectroscopy (XPS) and x-ray induced Auger electron spectroscopy (XAES) which are methods offering a wealth of spectral information. To calculate the electron charge transfer, we used XPS and XAES data in the form of the Auger parameter (AP), [8] in conjunction with the Thomas and Weightman model [9]. For a metal, such as Al, the Thomas and Weightman model can be simplified by assuming perfect local screening. However, for a dielectric material, such as Si, no simplification can be assumed and imperfect screening has to be implemented in the calculations. When calculating the charge transfer for a combined material of aSi and Al, the atomic potentials which influence the atomic structure and subsequently the optoelectronic properties of the aSiAl solutions have to be included in the calculations. This has been done by comparing the charge transfer calculations based on both screening models into the Thomas and Weightman model and then compare them to compare with density functional theory (DFT) calculations of the same system.

2. Methodology

aSiAl and aSiAl:H films have been deposited on mono-crystalline p-type Si (100) substrates by a CVC 601 magnetron sputtering equipment. Prior to deposition, the samples were etched by 1% HF solution for one minute to remove the native oxide from the substrate surface. The sputtering was carried out in an Ar atmosphere at a working pressure of 3 mTorr, with a power of 400W. Using a two-phase Al-Si target, uniform aSiAl films with Al content up to 25 at.% were produced. The hydrogenated samples were made by introducing hydrogen into the chamber during sputtering.

XPS was performed in a KRATOS AXIS ULTRA^{DL} instrument using monochromatic Al K α radiation ($h\nu = 1486.6$ eV). The x-ray source was operated at 10 mA and 15 kV, and high resolution spectra were acquired with a step size of 0.1 eV and pass energy between 10 and 40. The spectra were fitted with the computer program CasaXPS [10].

DFT calculations at the PBE-GGA level [11] and DFT-based molecular dynamics (MD) were performed using the Vienna *ab initio* simulation package (VASP) [12, 13]. The starting models were square supercells with $a = 10.932$ Å containing 1) 49 Si atoms + 15 Al atoms and 2) 58 Si atoms + 6 Al atoms. To create amorphous Si-Al structures MD was ran in 50 cycles of 200×1 fs at 5000 K. In between the MD cycles DFT relaxation of the cell volume was performed. After introducing structural randomness at elevated temperature, a third model was made where 12 H atoms were placed into model 2 at random. The three models were labelled Si58Al6, Si58Al6H12 and Si49Al15, to reflect the type and number of atoms in each cell. All models were MD quenched in two steps, adapted from the method used for pure Si by Jarolimek *et al* [14] From 2370 to 1818 K, approaching the solidification temperature of Si, the cooling rate was 0.138 K fs⁻¹, while from 1818 to 300 K the cooling rate was decreased to 0.023 K fs⁻¹. Model 1 was made in several versions to check the reproducibility of the results. After quenching, the atomic and electronic structure was relaxed using DFT to investigate the effect of increasing the Al content. The plane-wave energy cut-off was 500 eV and a Monkhorst-pack sampling of $5 \times 5 \times 5$ k-points was used to model the Brillouin zone. The break condition for the crystal structure relaxation loop was set to forces < -0.05 eV Å and the criterion for energy convergence was a change of the total energy less than 10^{-6} eV. Bader analysis [15] was used in order to investigate trends in charge transfer between Si and Al upon alloying. As DFT in general calculates the electron structure of the unit cell as a whole, individual atoms are not well defined in terms of associated charge. In the Bader approach the atoms are confined in volumes with surface drawn perpendicular to the minima of the charge density calculated by DFT. This way most of the charge present in the structure can be included, unlike when using, e.g. spheres, which leaves the electrons in the voids between the spheres unaccounted for. To generate the charge densities used as input for the Bader analysis, the number of grid-points in the Fast Fourier transform mesh was increased until the total number of electrons counted by the Bader method was converged with the total number of electrons in the unit cell.

3. Results

As previously reported [7], the aSiAl:H film exhibit a homogenous amorphous structure of silicon alloyed with Al. Data on film composition, ellipsometry and optical measurements were presented in detail in our previous paper [7]. From the ellipsometry data, the dielectric constants were found at an energy of 0.7 eV (at the band gap). This is not the exact value of the finite dielectric function, but can be satisfactorily used to estimate differences between the samples. These values are included with other data in table 1.

XPS and XAES are based on excitation of core levels, and although core electrons are not directly involved in bonding, they respond to changes in the atomic environment and to associated charge transfer/redistribution phenomena via energy shifts of their spectral peaks. XP spectra of the Si 2p,

Table 1. The average band gap (from UV-vis and ellipsometry) and dielectric constant from our previous paper [7]. Al 2p and Si 2p binding energies (E_b), the final state AP (α^*), and the change in final state AP ($\Delta\alpha^* = \alpha_{\text{aSiAl-alloy}}^* - \alpha_{\text{aSi}_{\text{int.}} \text{ or Al}_{\text{int.}}}^*$) relative to the reference value for Al [19] (1466.2 eV) and measured aSi. Change in total charge (Δq) on Si (e^-/atom) and Al (e^-/atom) site ($\pm 0.15 e^-/\text{atom}$) for the imperfect screening model (i.s.) and the perfect screening model (p.s.). Total charge per formula unit $\text{Si}_{(1-x)}\text{Al}_x$ is calculated from $(1-x)\Delta q^{\text{Si}} + x\Delta q^{\text{Al}}$.

Sample	Band gap ($0.1 \pm \text{eV}$)	Dielectric constant (ϵ at E_g)	E_b ($\pm 0.1 \text{ eV}$)		α_{Si}^* ($\pm 0.14 \text{ eV}$)	α_{Al}^* ($\pm 0.14 \text{ eV}$)	$\Delta\alpha_{\text{Si}}^*$ ($\pm 0.20 \text{ eV}$)	$\Delta\alpha_{\text{Al}}^*$ ($\pm 0.20 \text{ eV}$)	Imperfect screening $\Delta q_{i.s.}$			Perfect screening $\Delta q_{p.s.}$		
			Si 2p	Al 2p					Si	Al	Total charge	Si	Al	Total charge
aSi	1.35	12.25	98.70		1716.0		0							
$\text{Si}_{0.82}\text{Al}_{0.18}$	0.60	16.81	98.70	72.6	1716.1	1465.3	0.1	-0.9	-0.31	1.37	-0.01	-0.07	0.68	0.07
$\text{Si}_{0.75}\text{Al}_{0.25}$	0.65	16.81	98.70	73.7	1716.3	1465.2	0.3	-1.0	-0.44	1.52	0.05	-0.20	0.83	0.06
aSiH _y	1.85	8.41	98.70		1716.1		0.1		0.35		0.35	-0.07		-0.07
$\text{Si}_{0.92}\text{Al}_{0.08}\text{H}_y$	1.45	9.60	98.70	72.6	1716.0	1465.0	0.0	-1.2	0.25	1.84	0.38	0.00	0.91	0.07
$\text{Si}_{0.83}\text{Al}_{0.17}\text{H}_y$	1.30	11.56	98.70	72.8	1716.2	1465.1	0.2	-1.1	-0.08	1.67	0.22	-0.13	0.83	0.03

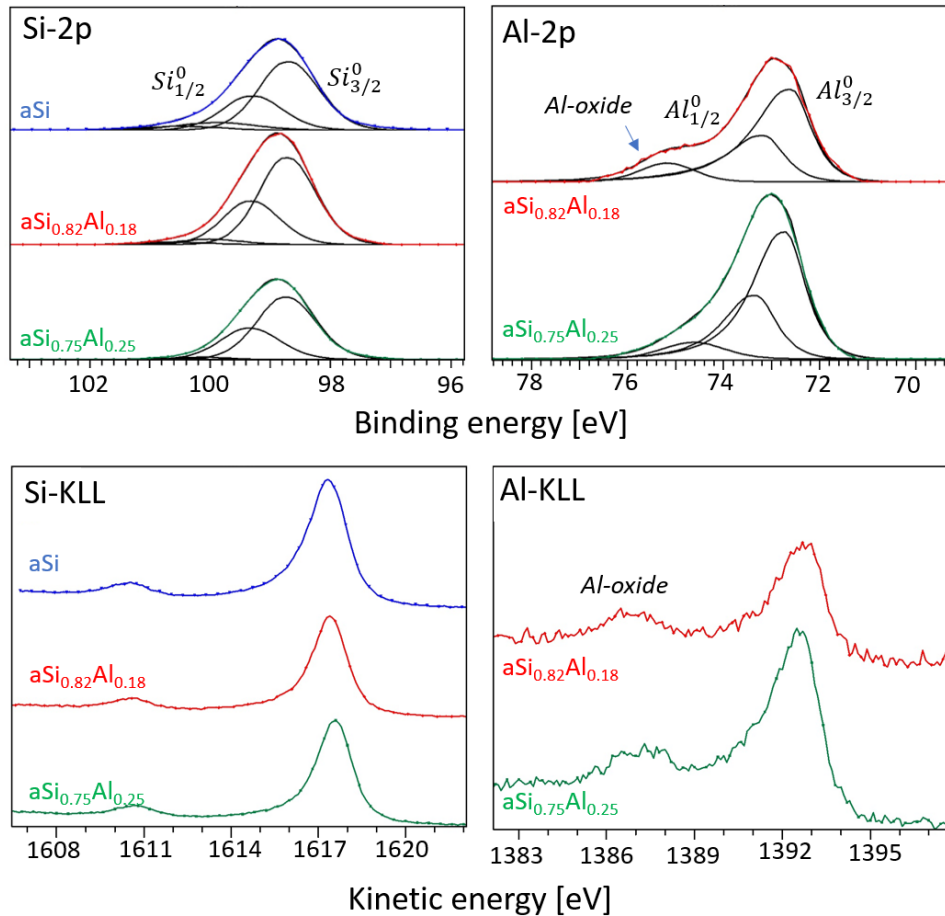


Figure 1. XPS spectra of the Al 2p, Si 2p, Al_{KLL}, and Si_{KLL} peak of the non hydrogenated films: aSi, Si_{0.82}Al_{0.18} and the Si_{0.75}Al_{0.25} film.

Al 2p, Si_{KLL}, and Al_{KLL} region from the non-hydrogenated and hydrogenated samples are presented in figures 1 and 2, respectively. The two main peaks fitted to the Si 2p spectra corresponds to elemental Si (Si⁰), the spin–orbit coupled Si_{3/2}⁰ and Si_{1/2}⁰ peaks. The Si 2p spectra have therefore been fitted with a Gaussian–Lorentzian function with a tail accounting for peak asymmetry (GL(30)T(6.5)) and a constant spin–orbit splitting of 0.6 eV. Likewise, two peaks corresponding to elemental Al has been fitted to the Al 2p spectrum with GL(70)T(1.4) and a constant spin–orbit splitting of 0.4 eV. The binding energies for the Si 2p and Al 2p peaks are presented in table 1. In addition to the Si⁰ and Al⁰ peaks, an oxide peak has been fitted to the Si 2p and the Al 2p spectra. The amount of Si⁺ present is around 10 ± 2 at.% in all samples, while only 3 ± 2 at.% for AlO_x.

In addition to the common practice of using core level energy shifts, we also measured and employed the modified final state Si and Al APs [9], and implemented them in the Thomas and Weightman model [9] in order to probe charge transfer phenomena upon alloying aSi with Al with/without H. In section 3.1 we use the spectroscopic results to investigate differences in core hole electron screening and interatomic charge transfer/re-distribution. In section 3.2 we present charge distribution calculations based on Bader analysis of

calculated DFT models, and in section 3.3 the experimental and computational results are compared.

3.1. Core hole screening and interatomic charge transfer

3.1.1. Variations in electron screening. Changes in final state Auger parameter (α^*) (AP) are defined as [9, 16]

$$\Delta\alpha^* = \Delta E_B + \Delta E_K \simeq 2\Delta R, \quad (1)$$

where ΔE_B and ΔE_K are the shift in photoelectron binding energy and the associated Auger electron kinetic energy, respectively, and ΔR represents the extra-atomic contribution to the relaxation energy. $\Delta\alpha^*$ is free of energy referencing problems and measures reliably the response of the material system to core hole electron screening [17, 18].

The AP results are presented in table 1. Upon alloying with Al, the Si 2p-*KLL* AP (α_{Si}^*) increases slightly with increasing Al content, as compared to pure aSi. At the same time, the Al 2p-*KLL* AP (α_{Al}^*) is significantly reduced compared to pure crystalline Al. α_{Al}^* does not appear to change much upon increasing Al content. A decrease of α_{Al}^* and an increase of α_{Si}^* in the aSiAl films, corresponds to a reduction in core hole screening of Al (compared to crystalline Al), and an increase of core hole screening of Si (compared to aSi) respectively.

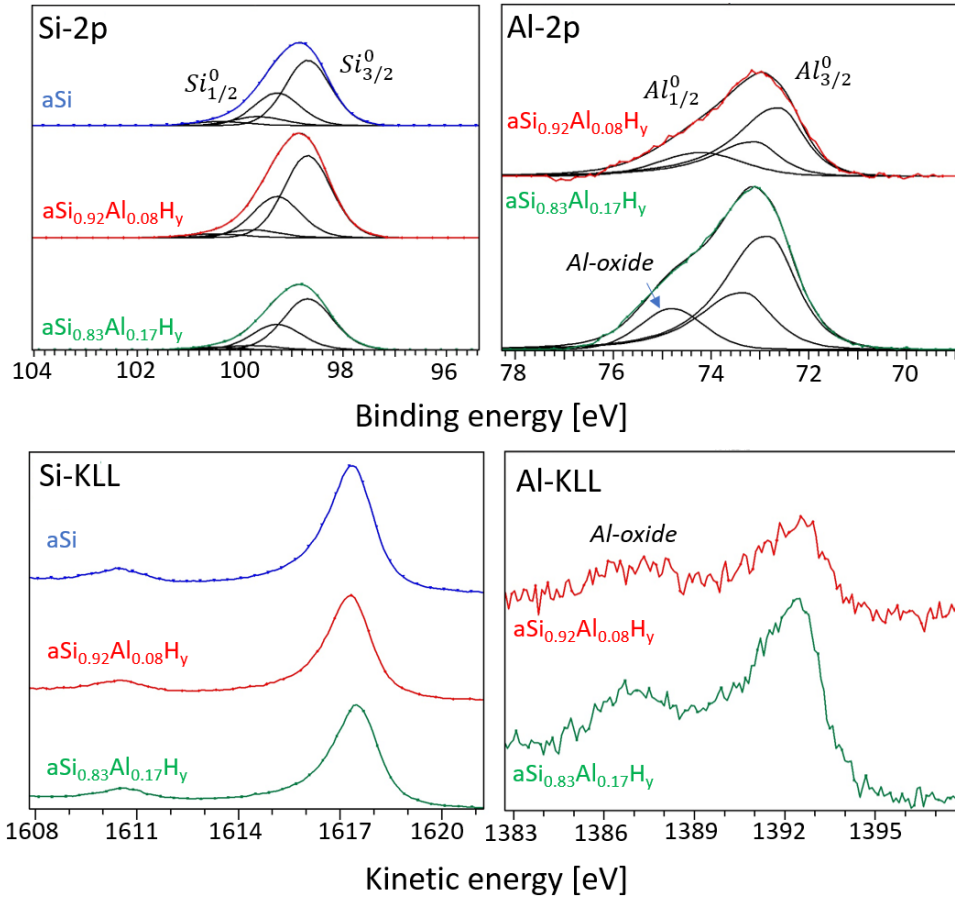


Figure 2. XPS spectra of the Al 2p, Si 2p, Al_{KLL}, and Si_{KLL} peak of the hydrogenated films: aSi_y, Si_{0.75}Al_{0.08}H_y and the Si_{0.83}Al_{0.17}H_y film.

When hydrogen is introduced, both α_{Al}^* and α_{Si}^* are slightly reduced, i.e. when comparing Si_{0.82}Al_{0.18} and Si_{0.83}Al_{0.17}H_y. The decrease of the AP, and subsequent reduction of the core hole screening, in the hydrogenated films could possibly be attributed to the formation of Al–H and/or Si–H bonds, where the electronegative nature of H results in electron transfer towards H.

The increase of the α_{Si}^* in the aSiAl films as compared to its value in aSi is in agreement with our observed reduction in the band gap of amorphous Si upon introduction of Al [7]. Although the slight changes in APs are close to or within the standard deviation, the measurements show a trend. The decrease in band gap of aSi upon alloying with Al relates to an enhanced screening on Si. The presence of a band gap in the aSiAl and aSiAl:H films stands as an energy barrier for the screening of the core holes of Al by the conduction electrons, and thus the α_{Al}^* values are much lower in the aSiAl and aSiAl:H films as compared to the metallic state where electron screening is perfect.

3.1.2. Interatomic charge transfer/distribution. The initial model of Thomas and Weightman [9] and its developed versions [8, 20] utilise variations in the AP ($\Delta\alpha^*$) between two chemical states e.g. between the elemental and the alloy state, in order to investigate charge transfer.

$$\Delta\alpha^* = \Delta\alpha_{\text{alloy}} - \Delta\alpha_{\text{element}}. \quad (2)$$

The α and $\Delta\alpha^*$ values of Al and Si in the investigated films are presented in table 1 whilst equation (3) below links $\Delta\alpha^*$ with changes in the valence charge q [9].

$$\Delta\alpha^* = \Delta\Sigma_i[q_i(\frac{dk_i}{dN}) + (k_i - 2\frac{2k_i}{dN})(\frac{dq_i}{dN})] + \Delta(\frac{dU}{dN}). \quad (3)$$

The above equation describes the linear potential model, where the potential in the core of an atom is assumed to vary linearly with the core occupation number N and the valence charge q of the atom. In equation (3) i refers to the valence orbital, and k reflects the change in the core potential when a valence electron is removed. The term dk_i/dN represents the shrinkage of the valence orbitals caused by the removal of a core electron; its sign is always negative. dU/dN , is the change in the atomic potential at the site due to changes in charge distribution of neighboring atoms caused by the creation of the core hole N [9].

Perfect metals, like Al, with an infinite dielectric constant are characterized by perfect local screening. Hence $(dq/dN) = 1$ in both chemical environments and subsequently $\Delta(dq/dN) = 0$. If we also assume that the polarization of the surroundings accompanying core-hole formation is zero for conductors, the above equation can be simplified to [9, 21]

Table 2. Average number of electrons (charge) per atom as calculated using Bader analysis, for different compositions. The relative charge is the difference in charge between the element in pure and alloyed state: positive (negative) values mean a decrease (increase) of electrons compared to elemental state.

Model	Element	Charge (e)	Relative charge (e)
Si58Al6	Si total	14.17	0.17
Si58Al6	Al total	11.39	-1.61
Si58Al6H12	Si total	14.06	0.06
Si58Al6H12	Al total	11.38	-1.62
Si58Al6H12	H total	1.54	0.54
Si49Al15	Si total	14.43	0.43
Si49Al15	Al total	11.58	-1.42

$$\Delta\alpha^* = \Delta q \left(\frac{dk}{dN} \right). \quad (4)$$

Equation (4) was therefore used to calculate change in charge on the Si and Al site using the perfect screening model. However, due to the dielectric properties of silicon, and of the Al–Si films (which show a band gap), it is necessary to also test the imperfect screening model. The imperfect screening model has been described by Waddington *et al* [20] as the Jost cavity model. It explains charge transfer when an ionized atom is placed in the center of a spherical cavity of radius R in a medium of dielectric constant ϵ [8]. The screening charge per core hole transferred to the Si-site from the atomic environment is therefore approximately $(1 - 1/\epsilon)e$ rather than ϵ , as assumed above [22]. With this approximation, the second and third term in equation (3) are important and the equation can then be reduced to the following form:

$$\Delta\alpha^* = \Delta q \left(\frac{dk}{dN} \right) + \Delta(1/\epsilon) \left[k - 2 \left(\frac{dk}{dN} \right) \right] \quad (5)$$

where $\Delta(1/\epsilon)$ reflects the difference in the finite dielectric constant between the semi-conducting element and the alloy under consideration: [22]

$$\Delta(1/\epsilon) = \frac{1}{\epsilon_{\text{alloy}}} - \frac{1}{\epsilon_{\text{element}}}. \quad (6)$$

The k and $\frac{dk}{dN}$ values for Si and Al are shown in table 1 in the supplementary material available online at stacks.iop.org/JPhysCM/30/335502/mmedia. In order to also calculate the charge transfer using the imperfect screening model for Al, the change in the core potential value (k) had to be calculated, since it was not available in literature. The k was calculated using the following equation [23]

$$k(q, N) = a + bN_c + cN_c^2 + (d + eN_c)q \quad (7)$$

where the parameters a , b , c , d and e are atomic potentials. These parameters can be determined from atomic structure calculations. The values we used in our calculations are from Jackson, Gregory, and Weightman [24], and they are shown together with the values for k in table 1 in the supplementary material. The average value between relaxed and excited states used was 11.91 eV for Si and 10.70 eV for Al. Using the k

and (dk/dN) values in table 1 in the supplementary material, the changes in AP ($\Delta\alpha^*$) and dielectric constants in table 1, equation (3) can be solved for Δq (Si (e^-) and Al (e^-)). The total results are presented in table 1, while the results for each excitation (2p;3p and 2p;3s) can be found in table 2 in the supplementary material.

Table 1 shows the calculated total changes in charge for Si and Al using both the imperfect screening ($\Delta q_{i.s.}$) and the perfect screening ($\Delta q_{p.s.}$) model. The positive signs of the change in charge in table 1 mean electrons are donated/transferred away from the site, while the negative signs mean electrons are received/ transferred towards the site. Both the imperfect and the perfect screening models show that when alloying aSi with Al, Al donates electrons to Si. When the amount of Al in the aSiAl alloy is increased, more electrons are transferred towards Si. The electron donation from Al to Si is in agreement with Si being slightly more electronegative than Al. The Pauling electronegativities of H, Si and Al are 2.20, 1.81 and 1.61, respectively. Hydrogenation of Al–Si is associated with electron transfer away from Si sites (presumably towards hydrogen). This charge transfer in the hydrogenated samples is in agreement with the electronegativity value for hydrogen. In the hydrogenated sample with the highest Al content, Si_{0.83}Al_{0.17}H₃, the electron transfer per Al atom decreases. However, the electron transfer from Al is larger with hydrogen than without, for the samples with similar Al content.

Estimations of electron charge transfer associated with H can be made only indirectly as we do not have experimental data (i.e. AP data) for H. It is, however, reasonable for us to assume that a reduction in charge on both Si and Al sites imply electron transfer towards the hydrogen sites, even though we cannot measure it directly. If charge transfer took place only between Al and Si, and from a charge neutrality point of view, one would expect that the total charge should be zero. This seems to be the case for both hydrogenated and non-hydrogenated samples in the perfect screening model, but not for the the hydrogenated samples in the imperfect model. For these samples the imperfect model shows a reduction in electron density at both Al and Si sites.

3.2. Bader analysis of charge distribution

Bader analysis was carried out on the DFT models produced from molecular dynamics, as described in section 1, and compared to the charge transfer found experimentally using both the perfect and imperfect screening models. Due to the lack of symmetry in the amorphous structures, the local environment of each individual atom was evaluated based on the nearest neighbor (nn) configurations, i.e. the number and type of nearest neighbor atoms. An nn radius $< 2.8 \text{ \AA}$ was found to encompass both Si–Si bonds and the slightly wider Si–Al separations. In table 2 the average charge of Si, Al and H in the Si49Al15, Si58Al6 and Si58Al6H12 models are presented. The change in average charge per Si atom is different for the two models without H; $-0.17 e$ for Si58Al6 and $-0.43 e$ for Si49Al15. Thus a higher fraction of Al atoms leads to a higher number of electrons transferred to the Si atoms. These results

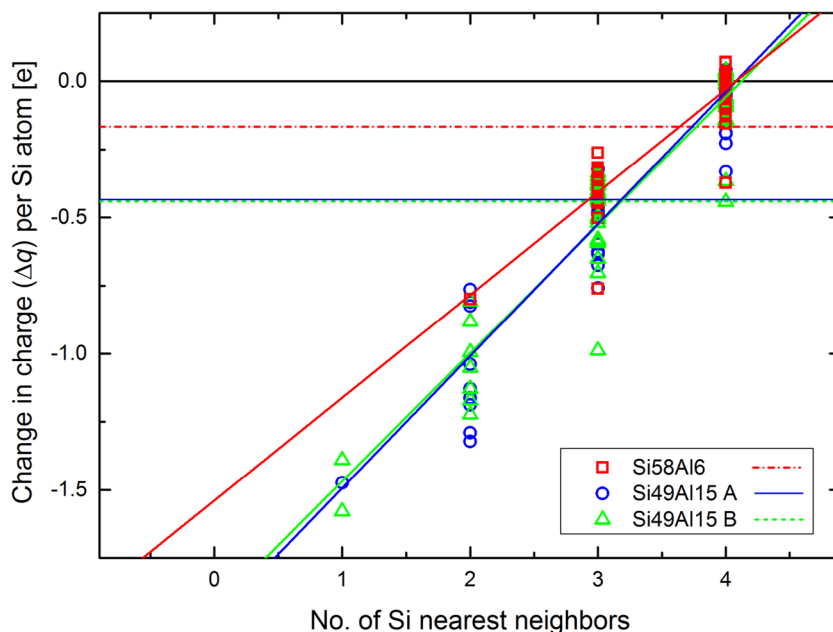


Figure 3. Change in charge (Δq) per Si atom, calculated using Bader analysis, as a function of number of nearest neighbor Al atoms for Si58Al6 (squares) and two of the Si49Al15 models (circles and triangles). Solid lines show the linear fit. The horizontal lines mark (from bottom to top) the average charge of Si in Si58Al6 and the average charge of Si in the two Si49Al15 models. The horizontal zero line corresponds to elemental Si.

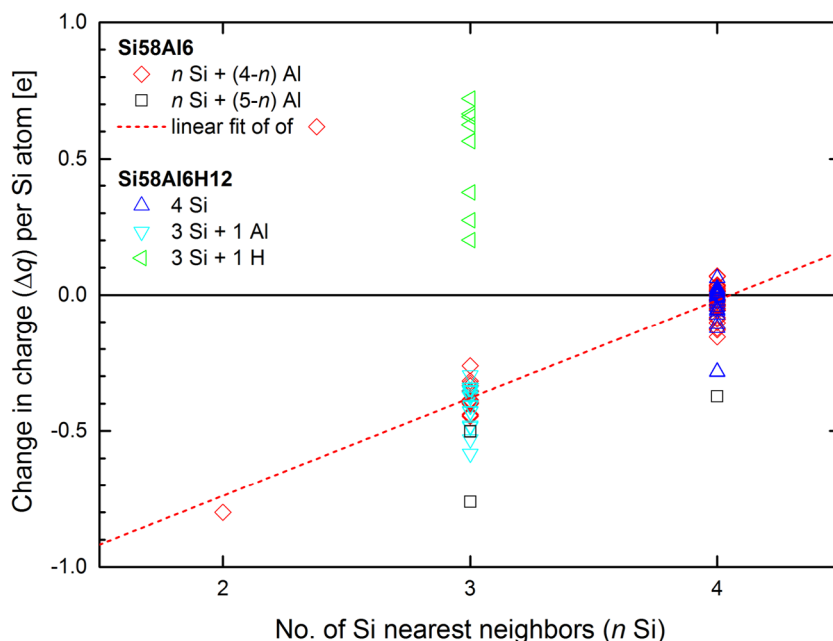


Figure 4. Calculated change in charge (Δq) per Si atom in the Si58Al6 and Si58Al6H12 models, as function of number of nearest neighbor Si atoms (n Si). Different nearest neighbor configurations are given different symbols, as labeled. The horizontal zero line corresponds to elemental Si.

suggests that alloying amorphous Si with Al is accompanied with a transfer of electrons from Al to Si, in agreement with our experimental results in 3.1.

The relation between the change in charge per Si atom and the number of Si nn can be fitted linearly, as shown in figure 3. The Si49Al15 models all show similar results, for clarity only two examples (labeled A and B) are shown in figure 3. Introduction of Al among the nearest neighbors of Si results in charge transfer between Al and Si, i.e. a decrease of electrons

per Al atom and an increase of electrons per Si atom. Si atoms with 4 Si and no Al atoms in the nn environment preserve a charge close to Si in the elemental state.

To investigate the effect of H, the change in charge per Si atom as a function of Si nn was compared for the Si58Al6 and Si58Al6H12 models in figure 4. For Si atoms with only Si or Si+Al among their nearest neighbors, the change in charge per Si atom is the same in both models, indicating transfer of electrons from Al to Si in both cases. For the Si

atoms with H among their nearest neighbors, however, electrons are transferred away from Si as well. Thus, upon introduction of H, electrons are directed towards H from both Si and Al, in agreement with their relative electronegativities. In average the number of electrons per H atom is increased, while the average number of electrons per Si atom ends up being equal to elemental Si in the model containing H. The average number of electrons per Al atom is reduced by the same amount regardless of whether or not H is present in the model.

In order to illustrate the distribution of electrons, selected charge density isosurfaces calculated for Si58Al6 and Si58Al6H12 are shown in figure 5. The lowest electron density is found in random areas with larger inter-atomic distances, as illustrated with isosurfaces drawn at $0.001 \text{ e} \text{ \AA}^{-3}$ (figures 5(a) and (c)). The highest electron density ($>0.09 \text{ e} \text{ \AA}^{-3}$ (figure 5(e)) is found inside Si–H and H–H bonds (examples labeled C and D, respectively), showing that H binds strongly to Si. When the isosurfaces are drawn at $0.07 \text{ e} \text{ \AA}^{-3}$ (figures 5(b) and (d)), Al–Si and Si–Si bonds (examples labeled A and B, respectively) appear. In the DFT model, H clearly prefers bonding to Si over bonding to Al, indicating a dependence of the average Si charge and the H content.

3.3. Comparison of XPS and DFT results

The results of the calculations for the Si49Al15 model have an Al content comparable to the real $\text{Si}_{0.75}\text{Al}_{0.25}$ sample. The calculated average change in charge per atom was $-0.43 e$ for Si and $-1.42 e$ for Al. This compares well to the experimental results obtained using the imperfect screening model, which gave a change in charge of $-0.44 e$ per Si atom and $1.52 e$ per Al atom. The perfect screening model, on the other hand, indicated far less charge transfer between Al and Si, with a change in charge of $-0.20 e$ per Si atom and $0.83 e$ per Al atom.

The calculated Si58Al6H12 model has an Al content comparable to the $\text{Si}_{0.92}\text{Al}_{0.08}\text{H}_y$ sample, and as far as transfer of electrons away from Al is concerned, the calculation and the experimental result obtained by using the imperfect screening model are in fair agreement (1.6 and 1.84 electron deficit per Al atom, respectively). For Si, on the other hand, the experiment indicates that electrons are being transferred away from Si as well (0.25 electrons lost per Si atom), presumably towards H, while in the calculations Si is neutral in terms of charge transfer. It is possible that the discrepancy could be due to differences in H content, as the H contents of the real samples are not known. In the calculated models, the average number of electrons transferred away from Al (1.60 e) is identical for the Si58Al6 and Si58Al6H12 models. Furthermore, the maximum charge loss found for Al in the Si49Al15 model is 1.57 e per Al atom, which may suggest that there is a maximum number of electrons that can be donated by Al. Thus for increasing the amount of H an increasing amount of electrons would have to be transferred from Si. For the real $\text{Si}_{0.83}\text{Al}_{0.17}\text{H}_y$ sample, Si seems to receive electrons (average change in charge $-0.08 e$) while the number of electrons transferred away from Al has slightly decreased (change in average charge 1.67 e), which

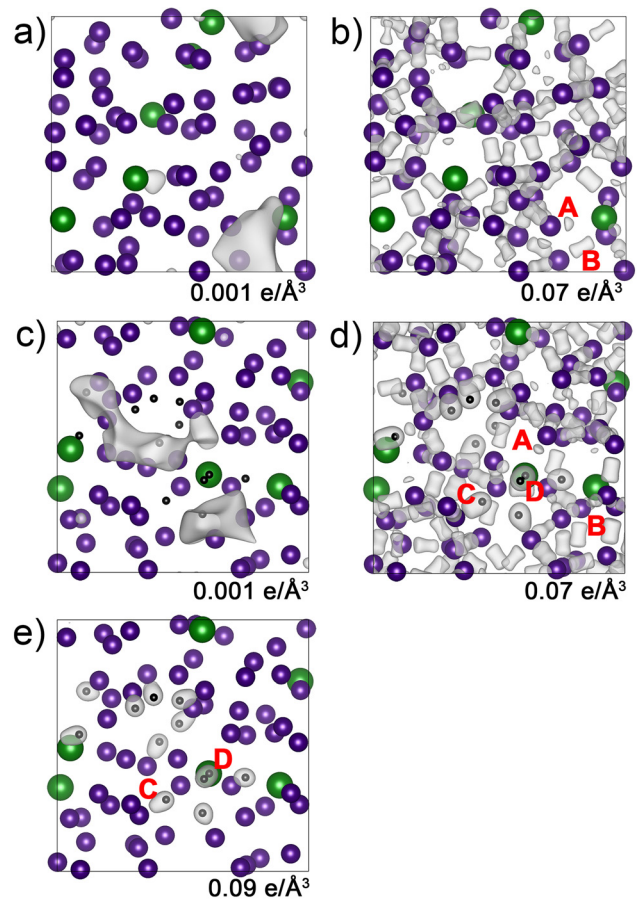


Figure 5. Calculated charge density isosurfaces for Si58Al6 (a) and (b) and Si58Al6H12 (c) and (e). Si atoms are illustrated using purple, medium size balls, Al atoms are big, green balls and H atoms are small, black balls.

is consistent with the argument above, i.e. that the increased amount of Al decrease the need for charge transfer from Si to H, assuming comparable H contents in the two samples.

The average change in charge per Si atom found experimentally from employing both the imperfect and the perfect screening model has been plotted in figure 6 together with the results from the DFT analysis. All the points from the DFT and imperfect screening results can be fitted to a line, showing a near perfect agreement. The results obtained by using the perfect screening model, on the other hand, show systematically less charge transfer. Thus the comparison to calculated results shows that when incorporating Al into a dielectric matrix, such as aSi, the imperfect screening model must be used when calculating the charge transfer. This fits well as Al is not a conductor in the $\text{aSi}_{1-x}\text{Al}_x\text{H}_y$ material, as in pure Al. Charge transfer calculated by the perfect screening model will then be reduced, as compared to the imperfect screening model. This is due to the loss of the last term in equation (5) which reflects the difference in the finite dielectric constant between the semi-conducting element and the alloy under consideration.

Based on the comparison to DFT, the experimental results obtained by using the imperfect screening model was chosen for further investigations of the relation between charge transfer and optical properties. In figure 7 the change in

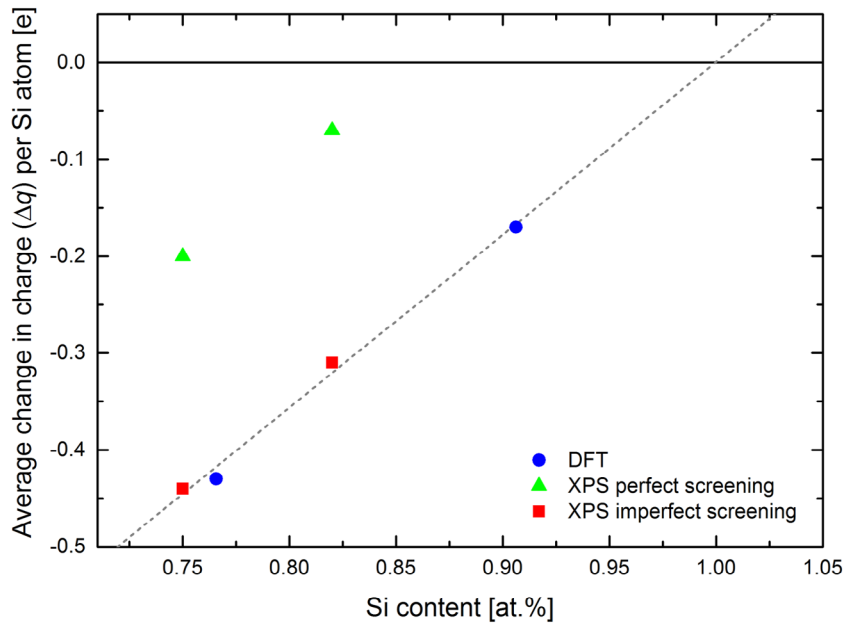


Figure 6. (a) Average change in charge (Δq) per Si atom as a function of Si content: DFT results for the Si49Al15 and Si58Al6 models (circles) and XPS results obtained for the Si_{0.75}Al_{0.25} and Si_{0.82}Al_{0.18} samples, using the perfect and imperfect screening models (triangles and squares, respectively).

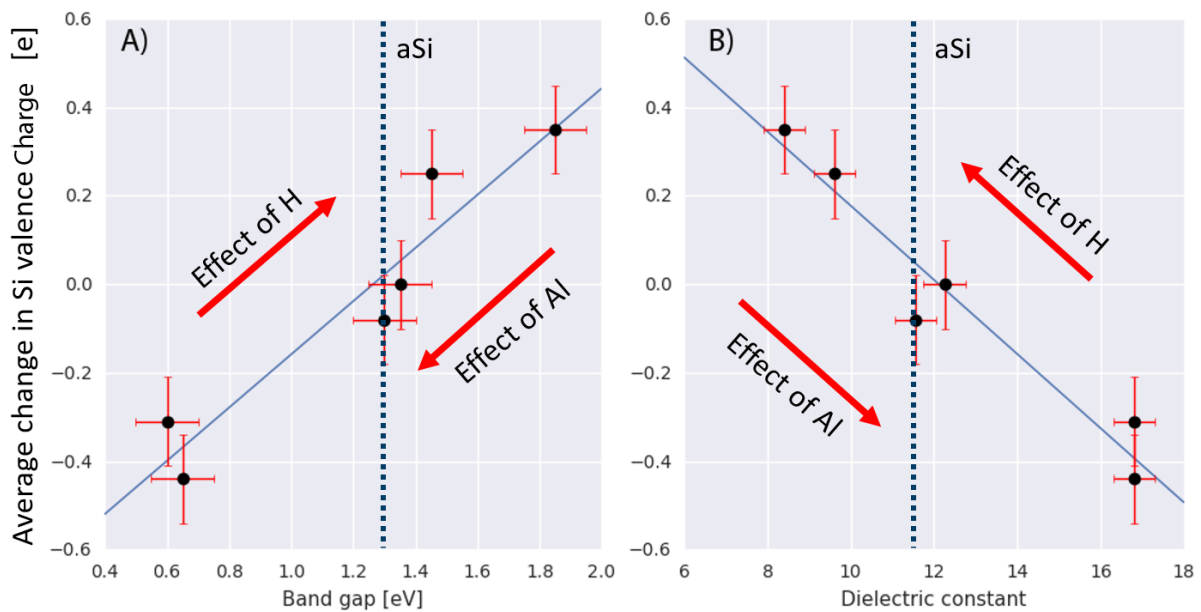


Figure 7. The valence of Si found by the interatomic charge transfer method found using the imperfect screening model, as a function of (A) the band gap, and (B) the dielectric constant found in our previous paper [7]. Data taken from table 1.

valence charge of Si was plotted as a function of band gap and dielectric constant (figures 7(a) and (b)), respectively). The graphs are made by using data from table 1. The linear trends in figures 7(a) and (b) summarize the effect of H and Al additions in aSi. Hydrogenation increases the E_g and reduces the dielectric constant of aSi, whilst at the atomic level reduces e^- density on the Si sites. Al has the opposite effect.

4. Conclusion

By calculating the change in total charge (Δq) from XPS results, we show that in Si_{1-x}Al_x thin films, electrons are

transferred away from Al and towards Si, in correspondence with the relative electronegativity values. When introducing hydrogen to form Si_{1-x}Al_xH_y, electron transfer is observed away from both Al and Si. The electrons can therefore be assumed to be transferred towards H. The experimental results were supported by DFT-based MD calculations, where a linear relationship was found between Si nearest neighbors and the number of electrons per Si atom. The number of electrons per Si atom increases (the valence of Si decreases) as the number of Al nearest neighbors increase. When H was introduced to the model, strong bonds were formed to Si, resulting in transfer of electrons from Si to H, while electrons were still transferred

from Al to Si. Our results also suggest that there is a maximum number of electrons that can be donated per Al atom. Thus, the measured change in average charge per Si atom will depend on the relative content of Si, Al and H in the sample.

Experimentally the valence of Si was found to have a linear relationship with the band gap, as well as with the dielectric function. The band gap increases when the valence of Si increases, while the dielectric constant decreases. The DFT results were compared to the values obtained experimentally using the Thomas and Weightman model, evaluating both the perfect and imperfect screening assumptions. From this comparison it became clear that the imperfect screening model has to be used in order to most accurately describe the charge of Al and Si when Al is incorporated into a dielectric matrix. It was shown that the average change in charge associated with the Si atom follows a linear trend with respect to the Si content. This means that the desired Si charge can be obtained by manipulating the alloying conditions.

Acknowledgment

This work is part of the project ‘Nanosol’, financially supported by the Research Council of Norway, grant no. 231658.

ORCID iDs

Annett Thøgersen  <https://orcid.org/0000-0002-4064-1887>

References

- [1] Ulyashin A, Scherff M, Hussein R, Gao M, Job R and Fahrner W R 2002 *Sol. Energy Mater. Sol. Cells* **74** 195
- [2] Jensen N, Rau U, Hausner R, Uppal S, Oberbeck L, Bergmann R and Werner J 2000 *J. Appl. Phys.* **87** 2639
- [3] Chopra L, Paulson P D and Dutta V 2004 *Prog. Photovolt., Res. Appl.* **12** 69
- [4] Barraud L et al 2011 *Appl. Phys. Lett.* **99** 123506
- [5] Galloni R 1996 *Renew. Energy* **8** 400
- [6] El-Naggar A H and Bakry A M 1999 *J. Phys.: Condens. Matter* **11** 9619
- [7] Thøgersen A, Jensen I T, Stange M, Røyset A, Røyset A, Ulyashin A and Diplas S 2016 *Appl. Phys. Lett. Mater.* **4** 036103
- [8] Evans J A, Laine A D, Weightman P, Matthew J A D, Woolf D A, Westwood D I and Williams R H 1992 *Phys. Rev. B* **46** 1513
- [9] Thomas T D and Weightman P 1986 *Phys. Rev. B* **33** 5406
- [10] CasaXPS, Casa Software Ltd. 2012 www.casaxps.com
- [11] Perdew J P, Chevary J A, Vosko S H, Jackson K A, Pederson M R, Singh D J and Fiolhais C 1992 *Phys. Rev. B* **46** 6671
- [12] Kresse G and Furthmüller J 1996 *Phys. Rev. B* **54** 11169
- [13] Kresse G and Furthmüller J 1996 *Comput. Mater. Sci.* **6** 15
- [14] Jarolimek K, de Groot R A, de Wijs G A and Zeman M 2009 *Phys. Rev. B* **79** 155206
- [15] Henkelmann A A G and Jónsson H 2006 *Comput. Mater. Sci.* **36** 354
- [16] Gaarenstrom S W and Winograd N 1977 *J. Chem. Phys.* **67** 3500
- [17] Walker C G H, Motron G B S A, Matthew J A D and Yousif F N 1994 *J. Electron Spectrosc. Relat. Phenom.* **70** 73
- [18] Matthew J A D, Morton S A, Walker C G H and Beamson G 1995 *J. Phys. D: Appl. Phys.* **28** 1702
- [19] Moulder J F, Stickle W F, Sobol P E and Bomben K D 1992 *Handbook of X-Ray Photoelectron Spectroscopy* (Eden Prairie, MN: Perkin-Elmer Corporation)
- [20] Waddington S D, Weightman P, Matthew J A D and Grassie A 1989 *Phys. Rev. B* **39** 10239
- [21] Weightman P, Cole R J, Brooks N J and Thornton J M C 1995 *NIM Phys. B* **97** 472
- [22] Arvanitis A, Diplas S, Tsakirooulos P, Watts J F, Whiting M J, Morton S A and Matthew J A D 2001 *Acta mater.* **49** 1063
- [23] Cole R, Gregory D and Weightman P 1994 *Phys. Rev. B* **49** 5657
- [24] Jackson M, Cole R, Brooks N and Weightman P 1995 *J. Electron Spectrosc. Relat. Phenom.* **72** 261